Electronic Supporting Information (ESI)

Photoelectrochemical properties of p-type $CuBi_2O_4$ prepared by spray pyrolysis of carbon-free precursor aqueous solution combined with post-annealing treatment

Kaisei Wakishima,[a] Tomohiro Higashi,[b] Akira Nagaoka,[a,c] and Kenji Yoshino*[a]*

[a] K. Wakishima, A. Nagaoka, and K. Yoshino, Electrical and Electronic Engineering Program, Faculty of Engineering, University of Miyazaki, 1-1 Gakuen-kibanadai-nishi, Miyazaki 889-2192, Japan.

[b] T. Higashi, Institute for Tenure Track Promotion, University of Miyazaki, 1-1 Gakuen-kibanadai-nishi, Miyazaki 889-2192, Japan.

[c] A. Nagaoka, Research Center for Sustainable Energy & Environmental Engineering, University of Miyazaki, 1-1 Gakuen-kibanadai-nishi, Miyazaki 889-2192, Japan.

*E-mails: t_higashi@cc.miyazaki-u.ac.jp , t0b114u@cc.miyazaki-u.ac.jp

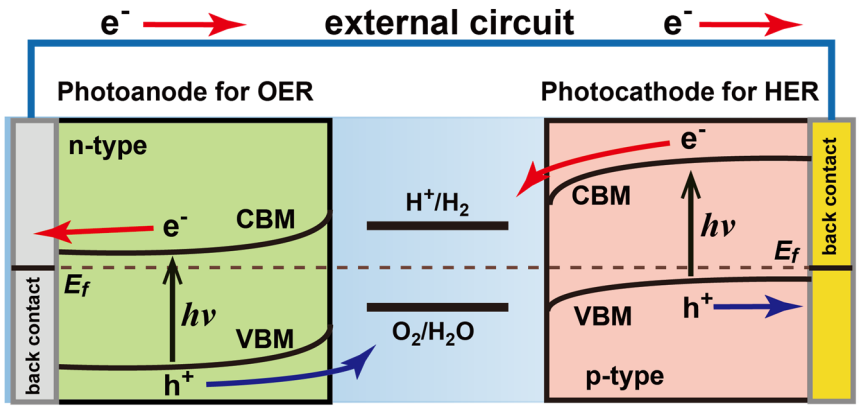

Figure S1. Schematic depiction of overall water splitting by the PEC cell comprising of the photocathode for HER and the photoanode for OER.

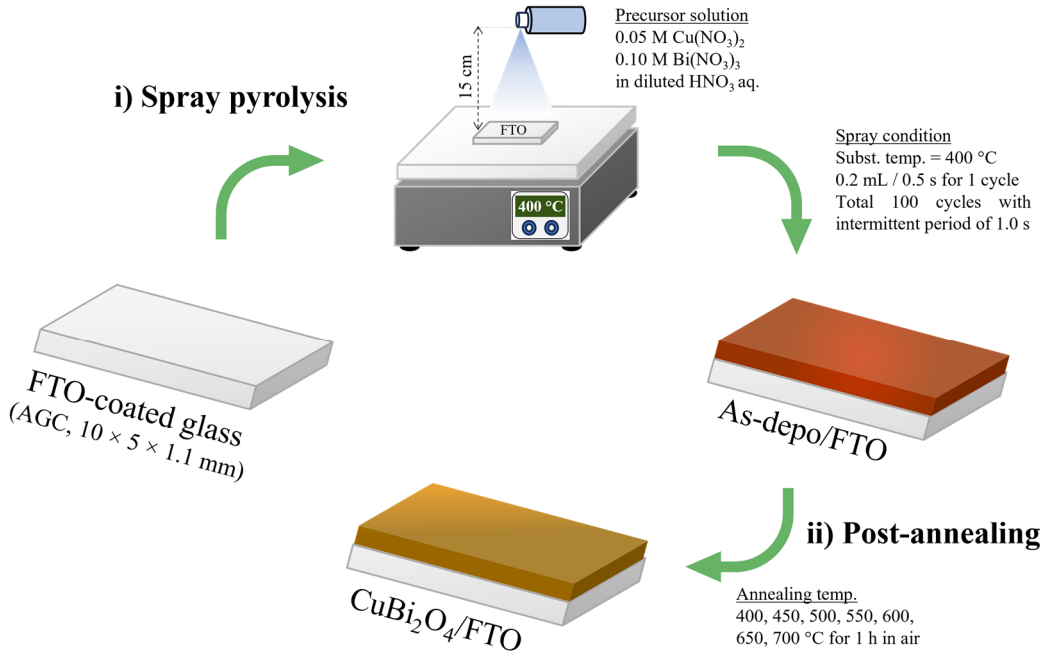

Figure S2. Fabrication process of $CuBi_2O_4$ thin film on FTO substrate.

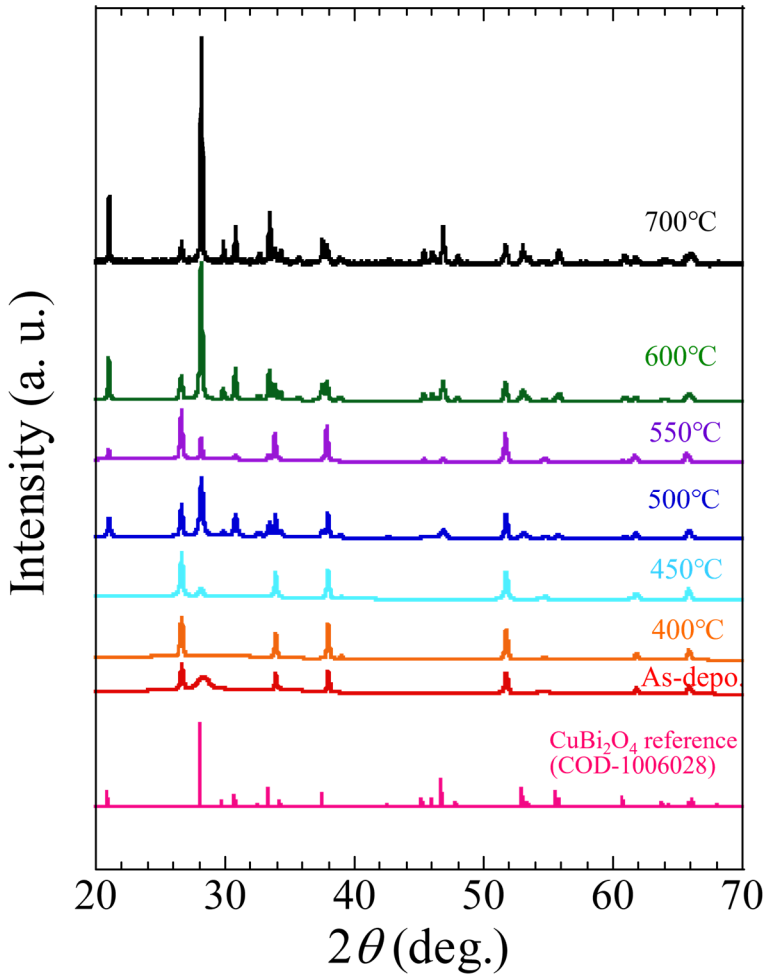

Figure S3. X-ray diffraction (XRD) patterns of the samples prepared through a spray pyrolysis (As-depo) and post-annealing treatment with different annealing temperatures of 400, 450, 500, 550, 600, and 700 °C for 1 h in air.

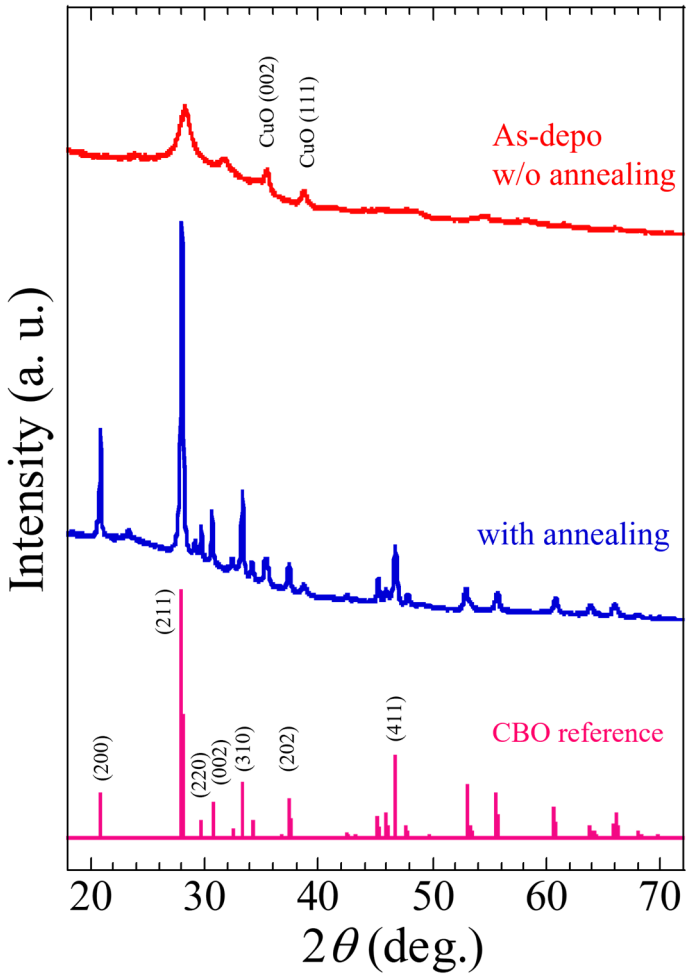

Figure S4. XRD patterns of the samples prepared on soda lime glass substrate (without an insertion of FTO layer) through a spray pyrolysis (As-depo) and post-annealing treatment at 600 °C for 1 h in air.

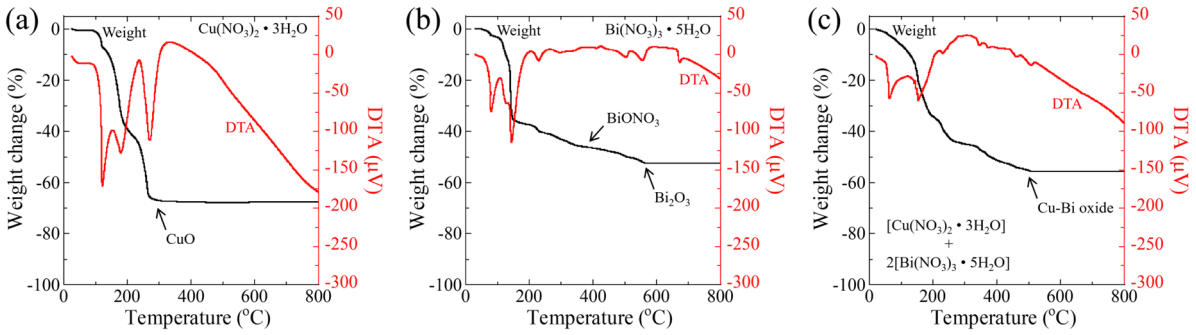

Figure S5. Thermogravimetry-differential thermal analysis (TG-DTA) data of (a) $Cu(NO_3)_2 \cdot 3H_2O$, (b) $Bi(NO_3)_3 \cdot 5H_2O$, (c) mixed powder of $Cu(NO_3)_2 \cdot 3H_2O$ and $Bi(NO_3)_3 \cdot 5H_2O$ with Cu : Bi = 1 : 2.

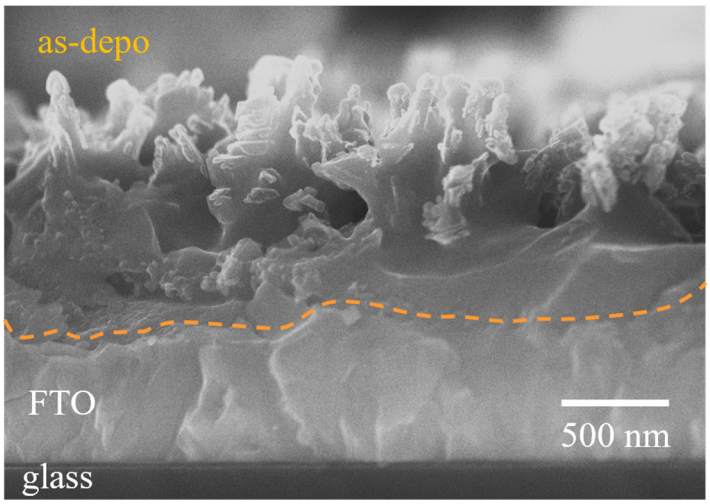

Figure S6. Cross-sectional SEM image for as-deposited film on FTO substrate.

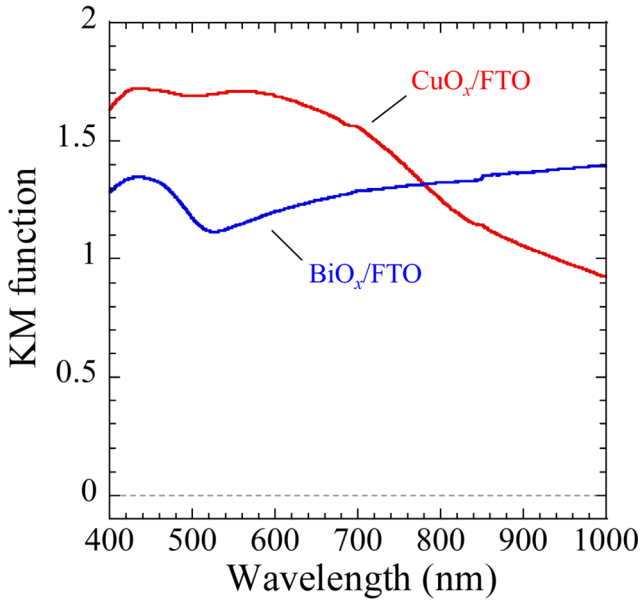

Figure S7. Diffuse reflectance spectra (DRS) of Cu-oxide (CuO_x) and Bi-oxide (BiO_x) prepared on FTO substrate through spray pyrolysis methods using the 0.05 M $Cu(NO_3)_2$ and 0.10 M $Bi(NO_3)_3$ dissolved in diluted nitric acid-based aqueous solutions. In the spray pyrolysis, the FTO substrate temperature was kept at 400 °C.

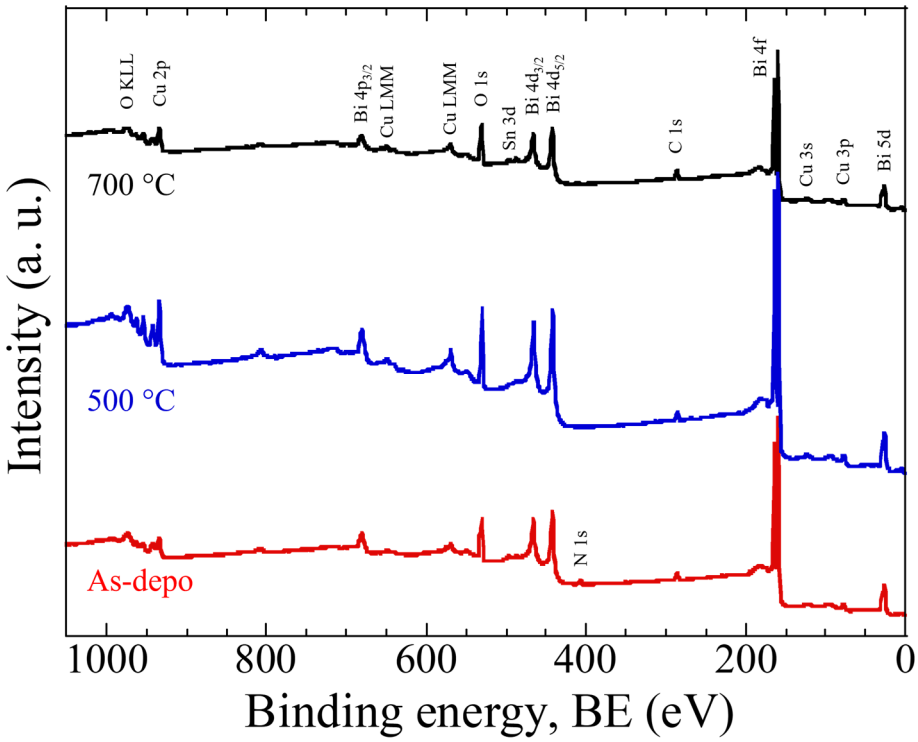

Figure S8. X-ray photoelectron spectroscopy (XPS) overall spectra (wide-scan XPS) of an as-deposited film on FTO (red), the samples processed by the post-annealing treatment at the temperature of 500 °C (blue) and 700 °C (black).

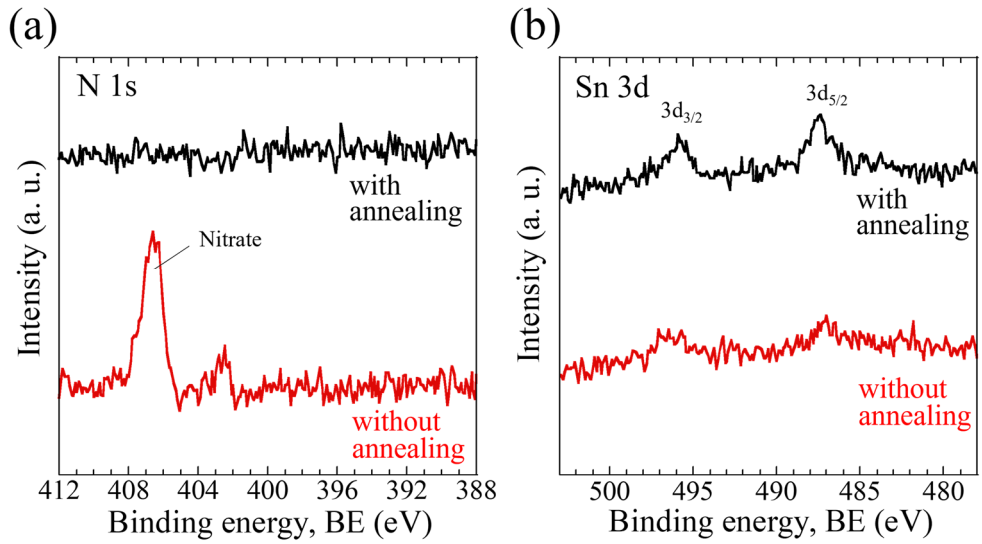

Figure S9. High-resolution XPS spectra of N 1s (a) and Sn 3d (b) for CBO samples with (colored in black) and without (colored in red) post-annealing treatment at 500 °C for 1h.

Table S1. Fitting parameters for HR-XPS Cu 2p spectra of CBO sample with a post-annealing treatment at 700 °C for 1 h in air

	Binding energy, BE (eV)		Full-width half maximum (eV)	
	Cu $2p_{3/2}$	Cu $2p_{1/2}$	Cu $2p_{3/2}$	Cu $2p_{1/2}$
Cu^{2+}	934.0	953.8	2.30	2.30
Reduced-Cu	932.4	952.2	1.10	1.10

Table S2. Surface concentration ratio of Cu^{2+} and Bi^{3+} from the HR-XPS spectra*

Annealing temp.	[Cu / (Cu + Bi)]	[Cu / (Cu + Bi)]	Cu^{2+} : Bi^{3+} **
w/o annealing	13.5 %	86.5 %	1.0 : 6.4
500 °C	19.2 %	80.8 %	1.0 : 4.2
700 °C	20.2 %	79.8 %	1.0 : 4.0

* Surface atomic concentration ratio of Cu and Bi of CBO samples was calculated using the results of HR-XPS peak fitting for the Cu 2p (Cu^{2+} peaked at 934.0 and 953.8 eV) and the Bi 4f (Bi^{3+} peaked at 158.8 and 164.1 eV) as shown in Figures 3a for Cu 2p and 3b for Bi 4f.

** Concentration ratio of Cu^{2+} and Bi^{3+} (Cu^{2+} : Bi^{3+}) was calculated using the ratio of [Cu / (Cu + Bi)] and [Bi / (Cu + Bi)] when we assumed the atomic concentrations of Cu and Bi are equivalent to the Cu^{2+} and Bi^{3+}, respectively.

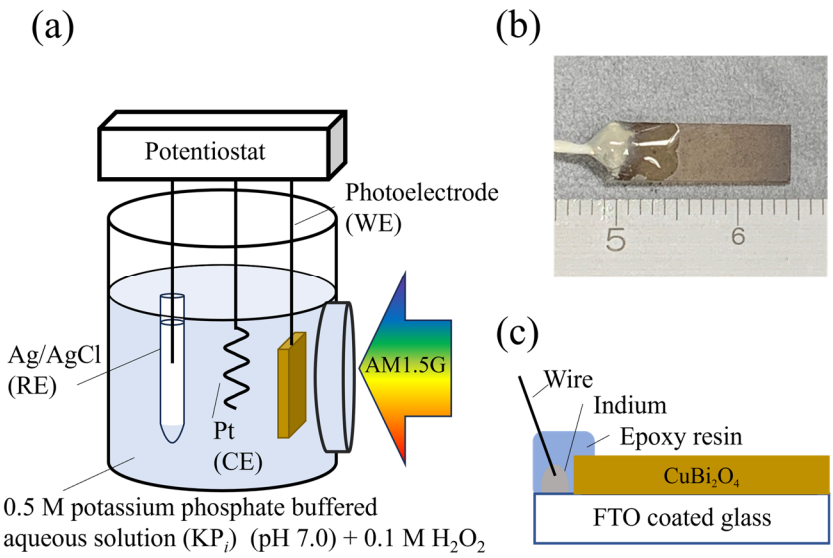

Figure S10. (a) Experimental set-up in a three-electrode configuration for the photoelectrochemical (PEC) measurements. (b, c) photograph and schematic of CBO-based photoelectrodes.

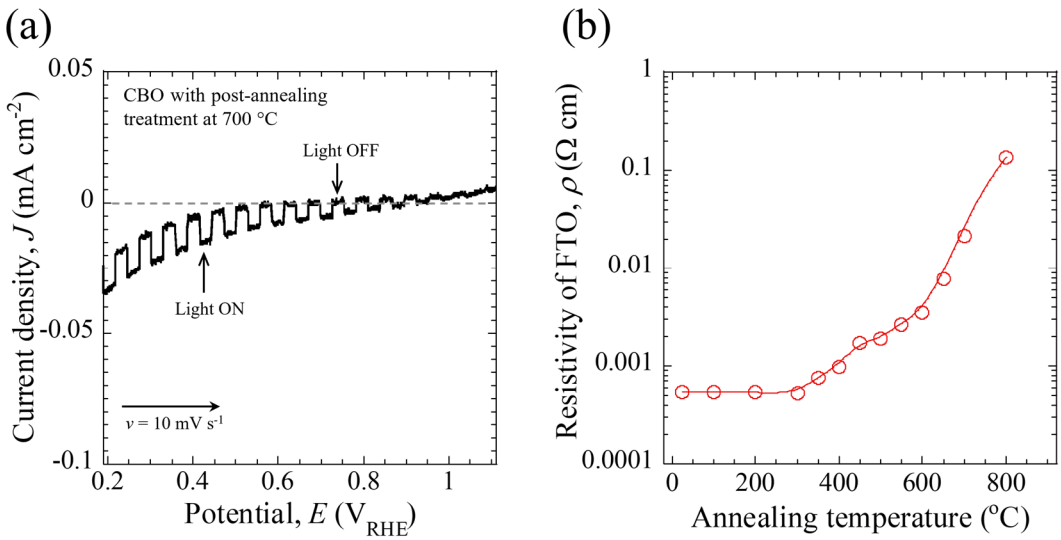

Figure S11. (a) Photocurrent density vs. photoelectrode potential (*J*–*E*) curve for the CBO-based photoelectrode processed with the post-annealing treatment at 700 °C for 1 h in air. The data was acquired in the 0.5 M KP$_i$ buffered aqueous solution with 0.1 M H_2O_2 sacrificial reagent (pH = 7.0) under chopped AM 1.5G solar illumination with a potential sweep rate (v) of 10 mV s^{-1}. (b) Plot of resistivity (r) of bare FTO substrate as a function of annealing temperature in air for 1 h.

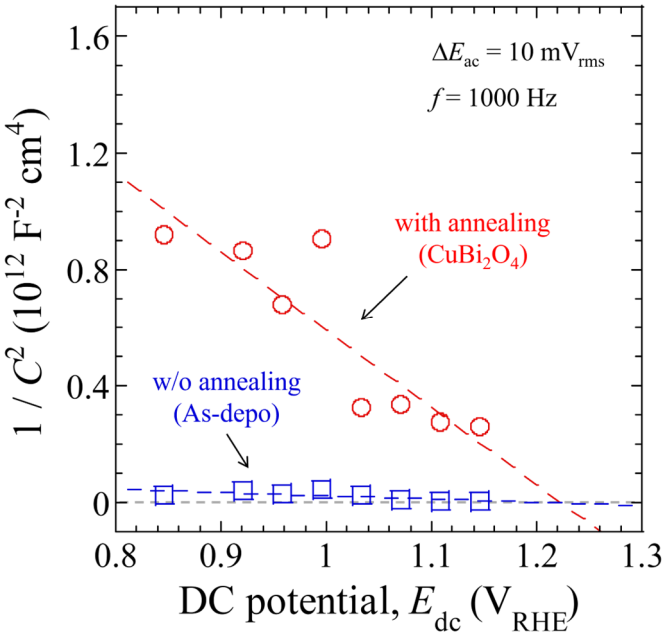

Figure S12. Mott-Schottky (MS) plot for CBO-based photoelectrodes with (circle) and without (square) post-annealing treatment. The data was acquired in a 0.5 M KP$_i$ buffered aqueous solution (pH = 7.0) in the dark condition. The CBO sample was annealed at a temperature of 600 °C for 1 h. The AC amplitude (ΔE_{ac}) and the frequency of potential modulation (f) were 10 mV_{rms} and 1000 Hz, respectively. The geometrical electrode area (A) of both photoelectrodes is 0.40 cm^2. The dashed lines indicate the fitting of the MS plot in the potential range from 0.85 V_{RHE} to 1.15 V_{RHE}. From the interception of the line with the x-axis (DC potential, E_{dc}), the flatband potential (E_{FB}) of CBO-based photoelectrode was calculated to be 1.20 V_{RHE}.

Table S3. PEC properties of CBO photoelectrodes processed by post-annealing treatment.

Annealing temperature (°C)	E_{on} (V_{RHE})*		J at 0.6 V_{RHE} (mA cm^{-2})	
	w/o H_2O_2	with H_2O_2	w/o H_2O_2	with H_2O_2
w/o annealing	0.64	0.86	–0.06	–0.34
400	0.64	0.92	–0.07	–0.44
450	0.65	0.96	–0.09	–0.57
500	0.74	1.04	–0.16	–0.92
550	0.74	1.04	–0.19	–0.94
600	0.76	1.06	–0.20	–0.94
650	0.73	0.97	–0.16	–0.58
700	–	–	–	–0.01

*Onset potential (E_{on}) was defined as the photoelectrode potential (V_{RHE}) required to generate a photocurrent density (J) of –0.05 mA cm^{-2}.

Table S4. Summary for the recently reported $CuBi_2O_4$ photocathodes prepared by wet processes.

	Preparation method	Electrolyte for PEC test	Photocurrent density, *J*	Ref.
Pt/CBO	Drop-casting	0.3 M K_2SO_4 (pH = 6.8)	–0.15 mA cm^{-2} at 0 V_{NHE}	[1]
Pt/CBO/CuO	Drop-casting	0.3 M K_2SO_4 (pH = 6.8)	–0.7 mA cm^{-2} at 0 V_{NHE}	[1]
CBO/FTO	Cathodically electrochemical deposition	0.1 M K_2SO_4 (pH = 6.8)	–0.23 mA cm^{-2} at 0.1 V_{RHE}	[2]
Pt/CBO	Electrodeposition	0.1 M NaOH (pH 12.8) saturated with O_2	–0.8 mA cm^{-2} at 0.6 V_{RHE}	[3]
Pt/Ag-CBO	Electrodeposition	0.1 M NaOH (pH 12.8) saturated with O_2	–1.0 mA cm^{-2} at 0.6 V_{RHE}	[3]
Pt/CBO	Drop-casting	0.3 M K_2SO_4 + 0.2 M phosphate buffer	–0.5 mA cm^{-2} at 0.4 V_{RHE}	[4]
CBO	Electrochemical Synthesis	0.1 M K_2SO_4 (pH = 10.8)	–0.07 mA cm^{-2} at 0.6 V_{RHE}	[5]
CBO	Electrodeposition	0.1 M K_2SO_4 (pH = 6.8)	–0.03 mA cm^{-2} at –0.4 $V_{Ag/AgCl}$	[6]
CBO/CuO	Electrodeposition	0.5 M Na_2SO_4	–0.9 mA cm^{-2} at 0.1 V_{RHE}	[7]
Pt/CBO/FTO	Thermal oxidation	0.3 M K_2SO_4/0.2 M phosphate buffer solution	–0.41 mA cm^{-2} at 0.3 V_{RHE}	[8]
CBO	Drop-casting	0.1M Na_2SO_4	–1.2 mA cm^{-2} at 0.15 V_{RHE}	[9]
CBO@MoS_2	Drop-casting	0.1 M NaOH	–0.182 mA cm^{-2} at 0.6 V_{RHE}	[10]
Pt/CBO	nanofiber fabrication process	0.1 M potassium borate (KB_i) buffer	–0.21 mA.cm^{-2} at 0.6 V_{RHE}	[11]
CBO	Drop-casting	0.1M Na_2SO_4	–3.0 mA cm^{-2} at 0 V_{RHE}	[12]
TiO_2/CBO	Electrodeposition	0.1 M NaOH	–0.35 mA cm^{-2} at 0.60 V_{RHE}	[13]
Textured-CBO	Vacuum Drop-casting	1 M NaOH (pH 13.6)	–1.77 mA cm^{-2} at 0.4 V_{RHE}	[14]

CBO	Spray pyrolysis	0.3 M K_2SO_4 + 0.2 M KP_i with H_2O_2 (pH = 6.65)	−2.0 mA cm^{-2} at 0.6 V_{RHE}	[15,16]
Gradient-CBO	Spray pyrolysis	0.3 M K_2SO_4 + 0.2 M KP_i with H_2O_2 (pH = 6.65)	−2.5 mA cm^{-2} at 0.6 V_{RHE}	[16,17]
STSA-CBO	Spray pyrolysis	0.3 M K_2SO_4 + 0.2 M KP_i with H_2O_2 (pH = 6.65)	−1.20 mA cm^{-2} at 0.6 V_{RHE}	[19]
Co-doped CBO	Spray pyrolysis	0.5 M Na_2SO_4 (pH = 7.2)	−1.6 mA cm^{-2} at 0.0 V_{RHE}	[20]
CBO	Spray pyrolysis	0.5 M KP_i (pH = 7.0)	−0.20 mA cm^{-2} at 0.6 V_{RHE}	This work
CBO	Spray pyrolysis	0.5 M KP_i with H_2O_2 (pH = 7.0)	−0.95 mA cm^{-2} at 0.6 V_{RHE}	This work

Table S5. Fabrication conditions of CBO/FTO photoelectrodes prepared by spray pyrolysis and thermal annealing and their PEC characteristics under AM1.5G solar illumination.

	Solvent and Additives	Substrate temp.	Post-anneal temp.	Electrolyte for PEC test	Photocurrent density, *J*	Ref.
CBO	Acetic acid/ethanol, PEG and TEOF	450 °C	–	0.3 M K_2SO_4 + 0.2 M KP_i (pH = 6.65)	−0.3 mA cm^{-2} at 0.6 V_{RHE}	[15]
CBO	Acetic acid/ethanol, PEG and TEOF	450 °C	–	0.3 M K_2SO_4 + 0.2 M KP_i with H_2O_2 (pH = 6.65)	−2.0 mA cm^{-2} at 0.6 V_{RHE}	[15,16]
Gradient CBO	Acetic acid/ethanol, PEG and TEOF	450 °C	–	0.3 M K_2SO_4 + 0.2 M KP_i with H_2O_2 (pH = 6.65)	−2.5 mA cm^{-2} at 0.6 V_{RHE}	[16, 17]
Pt/TiO_2/ CdS/CBO	Acetic acid/ethanol, PEG and TEOF	450 °C	–	0.3 M K_2SO_4 + 0.2 M KP_i (pH = 6.65)	−1.0 mA cm^{-2} at 0.0 V_{RHE}	[16]
RuO_x/TiO_2 /CdS/CBO	Acetic acid/ethanol, PEG and TEOF	450 °C	–	0.3 M K_2SO_4 + 0.2 M KP_i (pH = 6.8)	−0.22 mA cm^{-2} at 0.6 V_{RHE}*	[17]
RuO_x/TiO_2 /CdS/CBO	Acetic acid/ethanol, PEG and TEOF	450 °C	–	0.3 M K_2SO_4 + 0.2 M KP_i (pH = 6.65)	−0.33 mA cm^{-2} at 0.6 V_{RHE}**	[18]
RuO_x/TiO_2/ $BiVO_4$/CBO	Acetic acid/ethanol, PEG and TEOF	450 °C	–	0.3 M K_2SO_4 + 0.2 M KP_i (pH = 6.65)	−0.08 mA cm^{-2} at 0.6 V_{RHE}**	[18]

DA-CBO	Glacial acetic acid/ethanol	250 °C	550 °C	0.3 M K_2SO_4 + 0.2 M KP_i (pH = 6.65)	–	[19]
DA-CBO	Glacial acetic acid/ethanol	250 °C	550 °C	0.3 M K_2SO_4 + 0.2 M KP_i with H_2O_2 (pH = 6.65)	–0.13 mA cm^{-2} at 0.6 V_{RHE}**	[19]
TSA-CBO	Glacial acetic acid/ethanol	250 °C	550 °C	0.3 M K_2SO_4 + 0.2 M KP_i (pH = 6.65)	–0.05 mA cm^{-2} at 0.6 V_{RHE}**	[19]
TSA-CBO	Glacial acetic acid/ethanol	250 °C	550 °C	0.3 M K_2SO_4 + 0.2 M KP_i with H_2O_2 (pH = 6.65)	–0.50 mA cm^{-2} at 0.6 V_{RHE}**	[19]
STSA-CBO	Glacial acetic acid/ethanol	250 °C	250 °C and 550 °C	0.3 M K_2SO_4 + 0.2 M KP_i (pH = 6.65)	–0.13 mA cm^{-2} at 0.6 V_{RHE}**	[19]
STSA-CBO	Glacial acetic acid/ethanol	250 °C	250 °C and 550 °C	0.3 M K_2SO_4 + 0.2 M KP_i with H_2O_2 (pH = 6.65)	–1.20 mA cm^{-2} at 0.6 V_{RHE}**	[19]
Pt/ZnO /STSA-CBO	Glacial acetic acid/ethanol	250 °C	250 °C and 550 °C	0.3 M K_2SO_4 + 0.2 M KP_i (pH = 6.65)	–0.46 mA cm^{-2} at 0.4 V_{RHE}	[19]
CBO	Glacial acetic acid/deionized water	300 °C	500 °C	0.5 M Na_2SO_4 (pH = 7.2)	–0.6 mA cm^{-2} at 0.0 V_{RHE}***	[20]
Co-doped CBO	Glacial acetic acid/deionized water	300 °C	500 °C	0.5 M Na_2SO_4 (pH = 7.2)	–1.6 mA cm^{-2} at 0.0 V_{RHE}***	[20]
CBO	Diluted nitric acid/deionized water	400 °C	600 °C	0.5 M KP_i (pH = 7.0)	–0.20 mA cm^{-2} at 0.6 V_{RHE}	**This work**
CBO	Diluted nitric acid/deionized water	400 °C	600 °C	0.5 M KP_i with H_2O_2 (pH = 7.0)	–0.94 mA cm^{-2} at 0.6 V_{RHE}	**This work**

* *J* value was estimated from the IPCE spectrum.

** *J* value was estimated from the literature's linear sweep voltammograms (*J*-*E* curve).

*** The light source was a 300 W Xe lamp (100 mW cm^{-2}, $\lambda > 380$ nm).

We note that the mixing ratio of acetic acid to ethanol in references [15] through [20] is 1:9 (v/v), while the ratio of acetic acid to deionized water in reference [19] is 1:4 (v/v). $Cu(NO_3)_2$ and $Bi(NO_3)_3$ were dissolved into the acetic acid/ethanol solvent in references [15-19], while reference [20] used $Cu(CH_3COO)_2$ and $Bi(NO_3)_3$ for the starting material. A 1 vol% polyethylene glycol (PEG) and a 5 vol% trimethyl orthoformate (TEOF) were added to the acetic acid/ethanol (1:9 v/v) solvent (in references [15-18]).

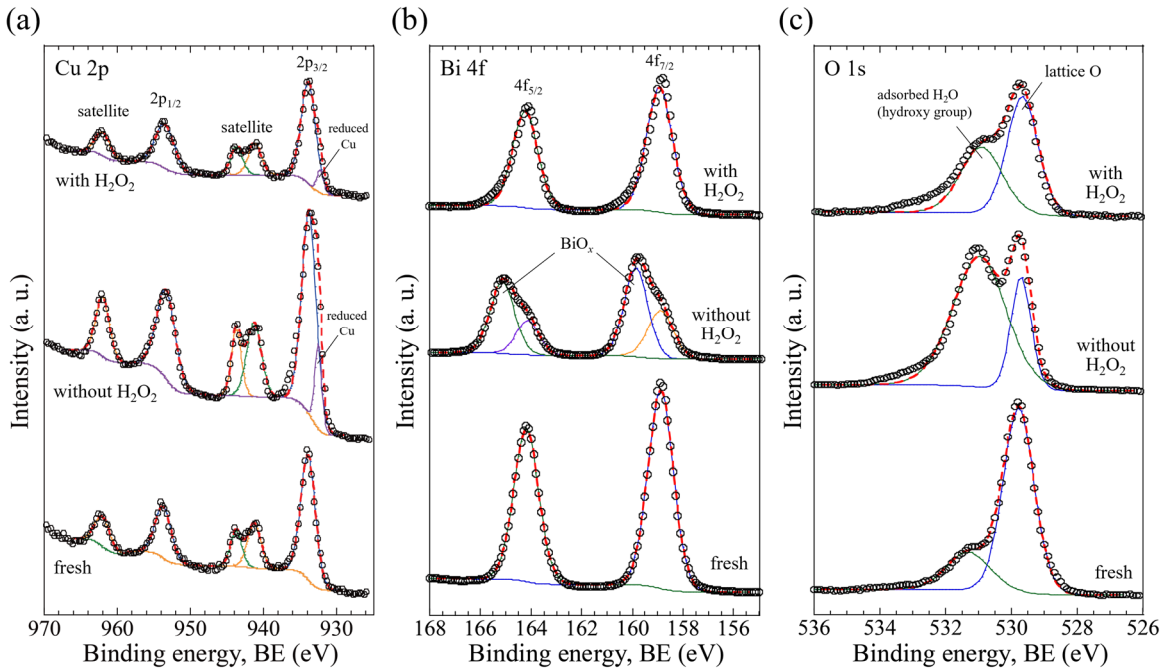

Figure S13. HR-XPS data for the CBO photoelectrodes before and after the PEC stability test at 0.6 V_{RHE} under simulated AM 1.5G solar illumination in the electrolyte contained with and without H_2O_2 sacrificial reagent. (a) Cu 2p, (b) Bi 4f, and (c) O 1s. Empty circles, solid lines (blue, green, orange, and purple), and dashed lines (red) indicate experimental data, fitted curves, and composite curves used in peak fitting, respectively.

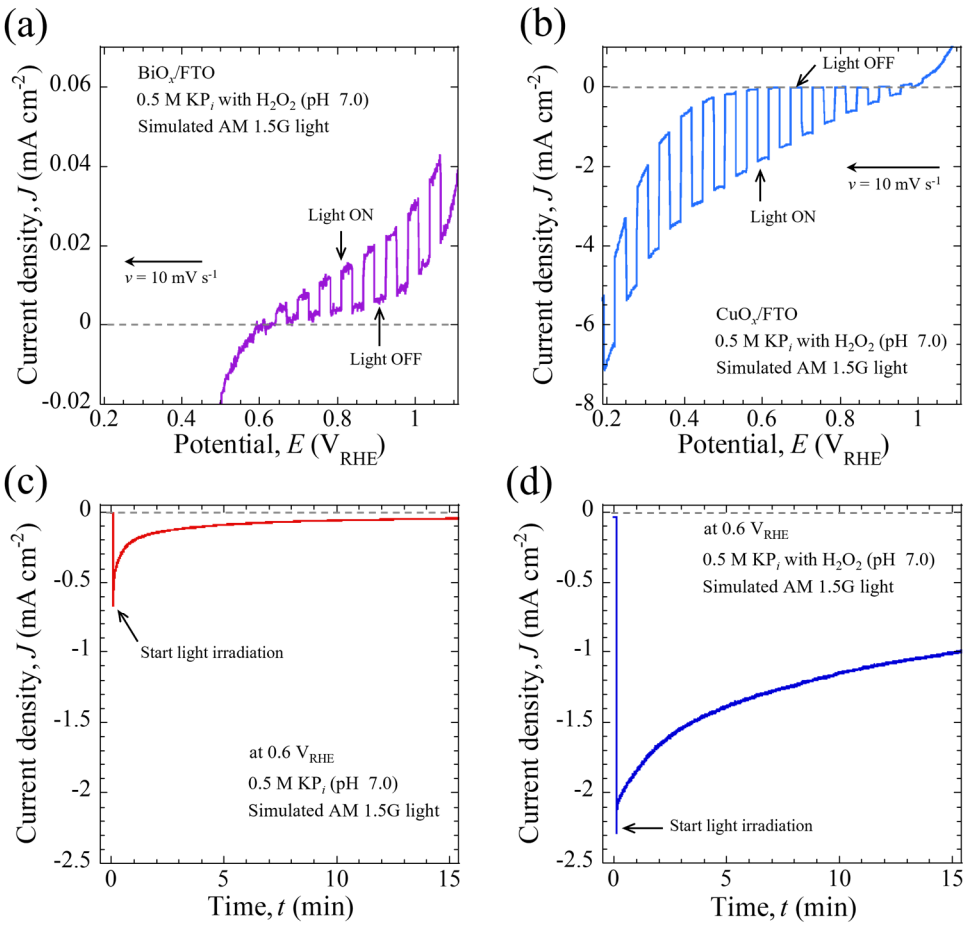

Figure S14. The PEC properties of BiO_x/FTO and CuO_x/FTO photoelectrodes. *J*–*E* and *J*–*t* curves for the BiO_x/FTO (a) and the CuO_x/FTO (b-d) photoelectrodes prepared via spray pyrolysis method at temperature of 400 °C using a dilute aqueous nitric acid precursor solution containing $Bi(NO_3)_3$ or $Cu(NO_3)_2$. The *J*–*E* curves were acquired in the 0.5 M KP_i buffered aqueous solution with 0.1 M H_2O_2 sacrificial reagent (pH = 7.0) under chopped AM 1.5G solar illumination with a potential sweep rate (v) of 10 mV s^{-1}. The *J*–*t* curves recorded at a constant *E* of 0.6 V_{RHE} were obtained in the 0.5 M KP_i aqueous solution without (c) and with (d) 0.1 M H_2O_2 sacrificial reagent.

Table S6. Summary of the stability test for CBO and CuO_x at constant E of 0.6 V_{RHE}.*

	Electrolyte**	$J_{t=1\ min}$ (mA cm^{-2})	$J_{t=15\ min}$ (mA cm^{-2})	$J_{t=15\ min}$ / $J_{t=1\ min}$
CBO	0.5 M KP_i	−0.19	−0.13	0.68
	0.5 M KP_i + H_2O_2	−0.94	−0.72	0.77
CuO_x	0.5 M KP_i	−0.18	−0.04	0.22
	0.5 M KP_i + H_2O_2	−1.85	−0.98	0.53

*The light source was simulated sunlight (AM 1.5G, 100 mW cm^{-2}).

**The electrolyte pH of potassium phosphate (KP_i) was adjusted to 7.0 by mixing of K_2HPO_4 and K_2HPO_4. The sacrificial reagent of H_2O_2 (0.1 M) was added to the KP_i buffered aqueous solution.

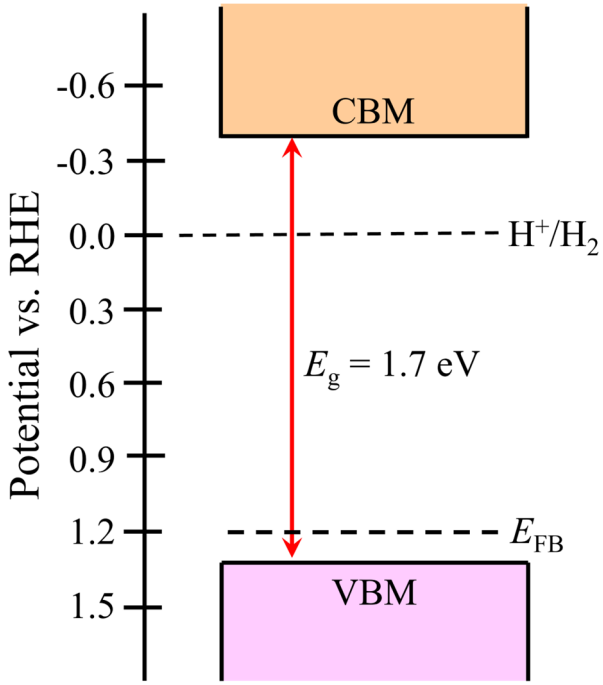

Figure S15. Schematic depiction of energy level diagram of p-type CBO. The diagram was based on the bandgap energy (E_g) of 1.7 eV and the flatband potential (E_{FB}) of 1.2 V_{RHE} delivered from the analysis of the Tacu plot (Fig. 5) and MS plot (Fig. S12).

References

[1] H. S. Park *et al*., *Phys. Chem. Chem. Phys*., **2014**, *16*, 22462- 22465.

[2] D. Cao *et al*., *J. Mater. Chem. A*., **2016**, *4*, 8995-9001.

[3] D. Kang *et al*., *Chem. Mater*., **2016**, *28*, 4331-4340.

[4] S. P. Berglund *et al*., *Chem. Mater*., **2016**, *28*, 4231-4242.

[5] N. T. Hahn *et al*., *J. Phys. Chem. C*, **2012**, *116*, 6459-6466.

[6] Y. Nakabayashi *et al*., *Electrochim. Acta*, **2014**, *125*, 191-198.

[7] S. Pulipaka *et al*., *J. Catal*., **2020**, *387*, 17-27.

[8] N. Xu *et al*., *Int. J. Hydrog. Energy*, **2018**, *4*, 2064-2072.

[9] M. Nishikawa *et al*., *Mat. Sci. Semicond. Proc*., **2017**, *57*, 12-17.

[10] K. Varunkumar *et al*., *Mater. Chem. Phys*., **2021**, *261*, 124245.

[11] X. Yuan *et al*., *Polymers*, **2021**, *13*, 3341.

[12] B. Meena *et al*., *Energy Fuels*, **2023**, *37*, 14280-14289.

[13] X. Zhu *et al*., C*hinese J. Catal*., **2018**, *39*, 1704-1710.

[14] J. Li *et al*., *Chem. Commun*., **2018**, *54*, 3331-3334.

[15] F. Wang *et al*., *J. Mater. Chem. A*., **2017**, *5*, 12838.

[16] F. Wang *et al*., *J. Am. Chem. Soc*., **2017**, *139*, 15094.

[17] A. Song *et al*., *ACS Appl. Mater. Interfaces,* **2020**, *12*, 13959.

[18] A. Song *et al*., *Chem. Sci*., **2020**, *11*, 11195.

[19] Y. Wang *et al*., *Int. J. Hydrog. Energy*, **2022**, *47*, 37774.

[20] C. G. O. Bruziquesi *et al*., *Int. J. Hydrog. Energy*, **2023**, *48*, 3456.